**EARTH'S CRYOSPHERE**
SCIENTIFIC JOURNAL

*Kriosfera Zemli*, 2020, vol. XXIV, No. 3, pp. 52–59 **http://www.izdatgeo.ru**

*PERMAFROST ENGINEERING*

DOI: 10.21782/EC2541-9994-2020-3(52-59)

# MODES OF TWO-PHASE CARBON DIOXIDE FLOW IN SOIL TEMPERATURE STABILIZATION SYSTEMS DEPENDING ON HEAT LOAD: AN EXPERIMENTAL STUDY

**V.P. Melnikov[1–4], G.V. Anikin[1,2], A.A. Ishkov[2,5], I.E. Andrianov[1,2], V.A. Gurtovoy[1]**

[1] *Autonomous non-profit organization "Provincial Academy", 86, Malygina str., Tyumen, 625026, Russia*
[2] *Earth Cryosphere Institute, Tyumen Scientific Centre SB RAS, 86, Malygina str., Tyumen, 625026, Russia; anikin@ikz.ru*
[3] *Tyumen State University, 6, Volodarskogo str., Tyumen, 625003, Russia*
[4] *Tyumen Industrial University, 38, Volodarskogo str., Tyumen, 625000, Russia*
[5] *Lukoil Engineering LLC, KogalymNIPIneft, 143A, Respubliki str., Tyumen, 625000, Russia; IshkovAA@tmn.lukoil.com*

During the experimental study of two-phase flow regimes of carbon dioxide in the systems of temperature stabilization of frozen soils, the condenser to evaporator flow pulsations were recorded under thermal loads on the evaporator below 2 kW (6.58 W/m). Results of the data processing for investigated pulsation modes allowed to determine the thermal boundary load at which the coolant pulsations at the condenser outlet are terminated.

*Two-phase flow, carbon dioxide, horizontal evaporator system, simulation*

## RELEVANCE OF THE RESEARCH

Resource development in Arctic and subarctic regions involves extensive works for site preparation and infrastructure construction on permafrost (e.g. roads, raw material storage facilities and other structures), thereby affecting natural soil temperature regime and causing partial melting of ice-rich ground.

Under conditions of thawing, strength properties of frozen soils tend to deteriorate, usually resulting in deformation and loss of bearing capacity of structures' foundations on which they are built [*Long, 1963; Farouki, 1986; Ershov, 1999; Holubec, 2008, 2010*]. The unwanted effects can be dealt with using specially designed temperature stabilization systems based on natural convection (thermosyphons) for seasonal cooling which cool the ground throughout the winter, while stop functioning during the summer [*Feklistov et al., 2008*]. Because of the specifics of their operation regime, these systems are also termed thermal (heat) diodes. Among major types of refrigeration systems capable to keep the ground frozen, this paper considers a system for ground temperature stabilization with horizontal evaporator tube (HET), or flat loop thermosyphon (Fig. 1).

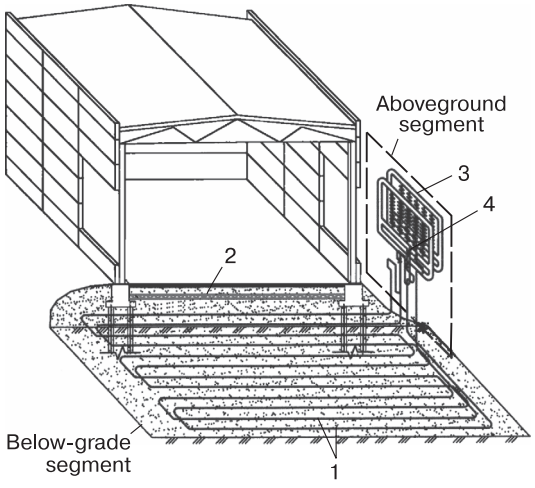


**Fig. 1. Thermal stabilization system with horizontal evaporator tubes [*Feklistov et al., 2008*]:**

1 – evaporator tubes; 2 – thermal insulation layer; 3 – accelerator pump; 4 – condenser.

The systems of this type which use ammonia as a working fluid (coolant) were developed by *FundamentStroiArkos* early in the 1990s and have become most widely used in Russia for construction in high latitudes to preserve and cool permafrost. This can be illustrated by the systems' involvement in the development of numerous oil/gas fields, which is corroborated by their amounts (in pieces), as follows: Vankor oil and gas field (560), Bovanenkovo gas field (289), Kharasavey gas field (175), Samburg fields (164), Novo-Urengoyskoe gas condensate field (127), Yurkhar oil and gas condensate field (104), etc. As of end 2018, a total of 2,222 ground temperature stabilization systems with a horizontal evaporator tube end were in use.

The installation procedure for these systems is described below. The evaporator tubes imbedded

within a granular layer (thermosyphon pad) allow the construction of buildings directly on the ground (slab-on-grade), while thermal insulation right above gravel layer with tubes, between evaporator and the building, prevents thawing of frozen ground during summer season, when the system is out of operation. The above ground surface condenser is in direct contact with ambient air, thereby dissipating the heat.

The coolant in the evaporator tubes in such a system is exposed to nucleate boiling at the ambient temperature lower than the ground temperature. The resulting vapor rises from the evaporator to the condenser located a few meters above the evaporator, where the vapor gives up heat to the air and condenses, and the condensed fluid gravitates back to the evaporator. Upon cooling in the evaporator tube, the working fluid changes from liquid to vapor (i.e. the cold air drops the pressure in the gas and thereby causes the fluid in the foundation to evaporate), while the system draws out the heat from below the building by a heat exchange mechanism; when the vapor condenses, heat is discharged into the atmosphere. The heat transfer from ground to the atmosphere thus provides for the ground freezing. The system operates only in winter (as long as the air temperature is colder than the ground). A layer of thermal insulation between the structure foundation and the evaporator serves to prevent the ground from thawing during the summer.

The experiments previously conducted on HET systems of this type used different gases as a coolant: acetone [*Gorelik, 2015*], ammonia [*Dolgikh, Okunev, 1989; Ishkov et al., 2018*] and propane [*Dolgikh, Okunev, 1989*]. The authors of this paper have studied this type of systems using carbon dioxide as working (fluid/gas) medium.

The proposed system can be likened to the experimental setup shown in Fig. 1, which includes a number of novel design characteristics and coolant ($CO_2$). The use of carbon dioxide as heat carrier was largely prompted by the research results discussed in [*Anikin, Spasennikova, 2014*] that theoretically proved it to be advantageous for such systems due to the least temperature difference between evaporator and condenser documented at the moment of the system starting. These systems begin to operate, once the ground becomes warmer than the atmosphere by as little as a few tenths of a degree (the temperature difference is almost zero), whereas the *Fundament-StroiArkos* designed systems (Fig. 1) which use ammonia as working fluid start operating, when the ground temperature becomes a few degrees warmer than the atmosphere. Consequently, the overwinter operating time of thermal stabilization systems using carbon dioxide is longer than that of systems using ammonia as coolant [*Anikin, Spasennikova, 2014*]. Thermal power of a system charged with carbon dioxide may be greater than the one charged with ammonia.

Let's consider the system , which is set by the expression:

$$W = \left(t_{con} - t_{air}\right) S\eta\alpha = \\ = \left(\left(t_{con} - t_{gr}\right) + \left(t_{gr} - t_{air}\right)\right) S\eta\alpha, \qquad (1)$$

where $W$ is thermal power of the system, the SI units are watts (W); $t_{con}$ is condenser temperature, °C; $t_{gr}$ is ground temperature at the interface with evaporator tube, °C; $t_{air}$ is air temperature, °C; $S$ is total area of the finned condenser section, $m^2$; $\eta$ is the coefficient of the efficiency of condenser fins; $\alpha$ is the coefficient of heat transfer of fins, $W/(m^2 \cdot °C)$.

The temperature difference ($t_{con} - t_{gr}$) equals $-0.53H$ for ammonia, and $-0.13H$ for carbon dioxide (where $H$ is the condenser height relative to the evaporator tubes, m) [*Anikin, Spasennikova, 2014*].

Then from (1) we obtain

$$W_{NH_3} = \left(-0.53H + \left(t_{gr} - t_{air}\right)\right) S\eta\alpha; \qquad (2)$$

$$W_{CO_2} = \left(-0.13H + \left(t_{gr} - t_{air}\right)\right) S\eta\alpha, \qquad (3)$$

where $W_{NH_3}$, $W_{CO_2}$ are the total heat (thermal power) of the system charged with ammonia and carbon dioxide, respectively.

By dividing the expression (2) by (3) and reducing the numerator and denominator by a value of ($t_{gr} - t_{air}$), we obtain

$$\frac{W_{CO_2}}{W_{NH_3}} = 1 - \frac{0.13H}{t_{gr} - t_{air}} \left[1 - \frac{0.53H}{t_{gr} - t_{air}}\right]^{-1}. \qquad (4)$$

Let's look at the behavior of the heat outputs of HET systems with a horizontal evaporator charged with different coolants ($CO_2$ and $NH_3$).

| $(t_{gr} - t_{air})$, °C | 2.65 | 3.0 | 4.0 | 5.0 | 10.0 |
|---|---|---|---|---|---|
| $W_{CO_2} / W_{NH_3}$ | ∞ | 6.71 | 2.48 | 1.85 | 1.27 |

At ($t_{gr} - t_{air}$) = 2.65 °C the system charged with ammonia will not work. Note that in the above calculations, the condenser (liquid column) height is assumed to be 5 m.

Noteworthy also is that thermal power of the system using carbon dioxide as working fluid is always greater, than the one using ammonia. Moreover, with a <2.65 °C difference between the ground temperature and ambient air temperature, operation of the system charged with ammonia is arrested completely, which is interpreted to be as the adverse effect of this coolant (Fig. 2).

The evaporator tubes of the proposed experimental setup are thermally insulated and heated by electric current, instead of being buried in the ground, which is the case with the systems described above. This allows to achieve specified heat loads, and to maintain the relationships between them and other parameters (coolant temperature, working fluid flow, vapor flow, etc.).

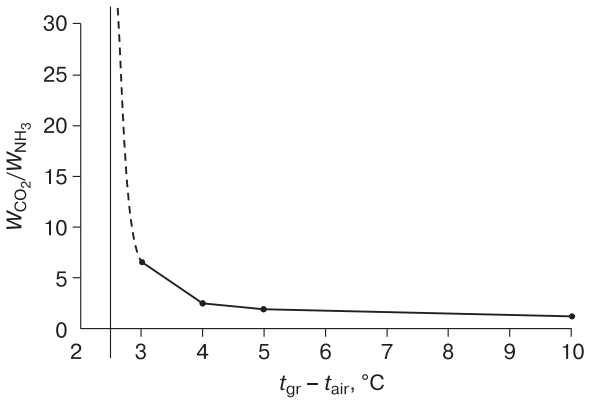


**Fig. 2. A relationship between heat outputs of systems using carbon dioxide and ammonia.**

Dashed line denotes extrapolation with respect to the considered values approaching the asymptote.

The research results have revealed some operation patterns of such thermosyphons and determined the ways of their improvement. It has been experimentally shown that the device having a large condenser surface area can operate at a temperature difference of <1 °C between the ground and atmosphere.

## DESIGN OF THE EXPERIMENTAL SETUP

The experimental setup (see Fig. 3 for its general view) is an air-tight construction where the evaporator is in flow communication with the condenser. The evaporator is a sealed steel tube 32 mm in diameter, with a wall thickness of 3 mm and a length of 304 m. The evaporator tube (diameter: 120 mm) is covered with thermal insulation (foamed polyurethane shell coating). The condenser consists of 48 interconnected finned tubes 102 mm in diameter (wall thickness: 4 mm). Each fin represents an aluminum square with 0.1 m sides. The area of finned section totals to 76.36 $m^2$.

The level of liquid in the condenser (which can be variable during the experiment) is marked by $y$ (Fig. 4). Given that the tube ending (the upward pointing arrow in Fig. 4) located at the condenser inlet is always higher than the level of liquid in the condenser, it acts as a hydraulic lock, ensuring liquid flow in a direction from the condenser inlet towards its outlet. The condenser is placed 3.1 m higher than the evaporator tubes.

In the experimental setup, the thermal load onto the evaporator unit is actuated by electric heater mounted along the tubes. This ensures a heat flux necessary for simulation of the operating procedure under conditions of thermal effect of structures built on permafrost. The electrical diagram (circuit) of the tube heater is shown in Fig. 5.

The evaporator tubes are powered from an alternating current supply via a step-down transformer. The transformer has two terminals: one connected to point A, and the other to points B. Since the condenser inlet and outlet have the same electrical potential, electric current does not run through the condenser.

The temperature of the evaporator tubes was measured by thermistors $T_1$, $T_2$ and $T_3$, placed at different segments of the evaporator: at the beginning, in the middle and at the end (Fig. 5). The temperature of the condenser fins was measured by thermistors $T_4$, $T_5$ and $T_6$ (Fig. 4), and the temperature of the ambient air was measured by thermistor $T_9$ located some distance from the system. The flow rate of liquid

**Fig. 3. General view of the thermal stabilization system (thermosyphon).**

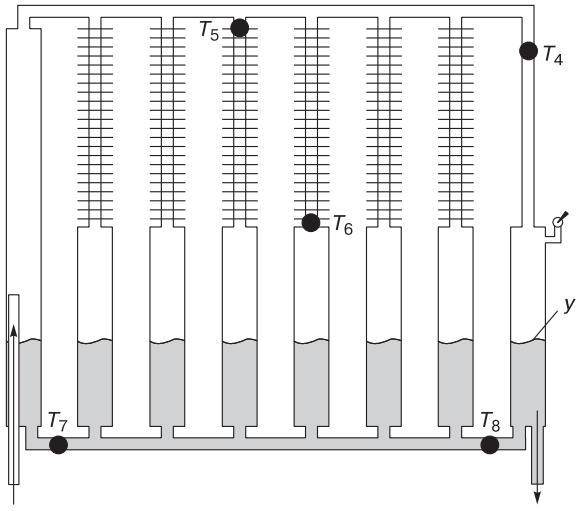


**Fig. 4. Level of working fluid ($y$) in the condenser.**
$T_i$ – thermistors.

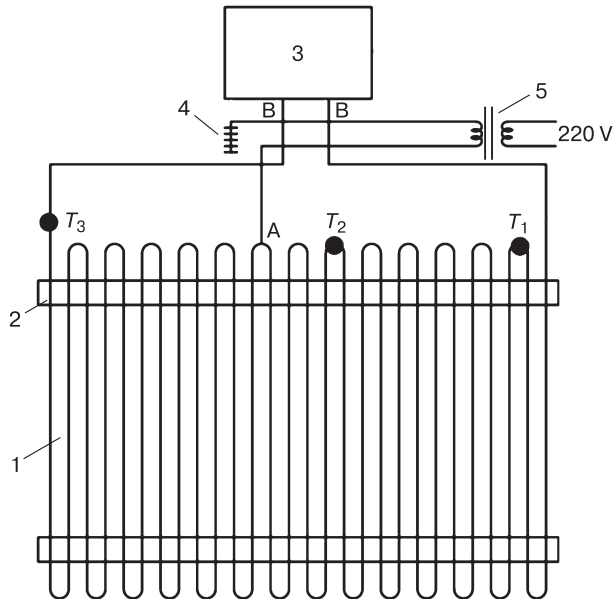


**Fig. 5. Top view of the system and tube heating circuit:**
1 – tubes with foamed polyurethane shell coating; 2 – thermosiphon pad; 3 – condenser; 4 – earthing; 5 – step-down transformer.

coolant at the condenser outlet was determined using the StreamLux SLS-700F ultrasonic flowmeter.

**Experimental setup operation under various thermal loads on the evaporator**

Results of the experiments which involved thermal loads below 2 kW (6.58 W/m) applied to the evaporator, reported fluid flow pulsations along the path from the condenser to the evaporator, which were investigated during a total of four runs with the thermal load values as low as: 0.734, 1.05, 1.51 and 2.05 kW.

Figure 6 shows that dependences of the fluid rate ($v$) at the condenser outlet are quasi-periodic, which therefore can be represented as Fourier series. Any periodic function $f(\tau)$ can be written, as follows:

$$f(\tau)=\frac{a_0}{2}+\sum_{n=1}^{\infty}\left(a_n\cos\left(\frac{2\pi n\tau}{T}\right)+b_n\sin\left(\frac{2\pi n\tau}{T}\right)\right), \quad (5)$$

where $T$ is the period of the function, and the coefficients $a_n$ and $b_n$ are set by the expressions

$$a_n=\frac{2}{T}\int_0^T f(\tau)\cos\left(\frac{2\pi n\tau}{T}\right)d\tau,$$
$$b_n=\frac{2}{T}\int_0^T f(\tau)\sin\left(\frac{2\pi n\tau}{T}\right)d\tau. \quad (6)$$

When decomposing the function shown in Fig. 6, *a* into a Fourier series, we consider three time values at which the graph of the function crosses the line $v = 0$ simultaneously decreasing. We thus obtain three values: $\tau_0 = 24.5$ min, $\tau_1 = 69$ min, $\tau_2 = 108.5$ min. The period containing the average peak is $T_1 = \tau_1 - \tau_0 = 44.5$ min. The period containing the rightmost peak is $T_2 = \tau_2 - \tau_1 = 39.5$ min. The visual representation resulting from the Fourier series expansion (5), (6) over a period containing the middle and right-hand peaks is shown in Fig. 7.

Henceforward, we have chosen a reference system showing the flow rate vector projection to be positive (i.e. working fluid flows from the condenser to the evaporator) or, conversely, negative (i.e. working fluid flows from the evaporator to the condenser). As it follows from Fig. 7, the obtained functions $f_1(\tau)$ and $f_2(\tau)$ describe the middle and right-hand spikes perfectly well.

Figure 8 shows a correlation between the approximating functions and the experimental data throughout the experiment.

These plots (Fig. 8) illustrate the function $f_2(\tau)$ describing the middle and rightmost spikes perfectly well, and $f_1(\tau)$ that describes the middle and leftmost spikes fairly adequately. The impossibility of providing an explication of all the peaks using a single function at a 0.734 kW thermal power indicates that during the experiment, their period and amplitude displayed shifts caused by variable external factors. Noteworthy is that such a small thermal loading would translate to instability of the transformer operation, which was likely responsible for the observed difference in the fluid flow rate at the condenser outlet.

In order to decompose the function shown in Fig. 6, *b* into a Fourier series, we consider three time values at which the function crosses the line

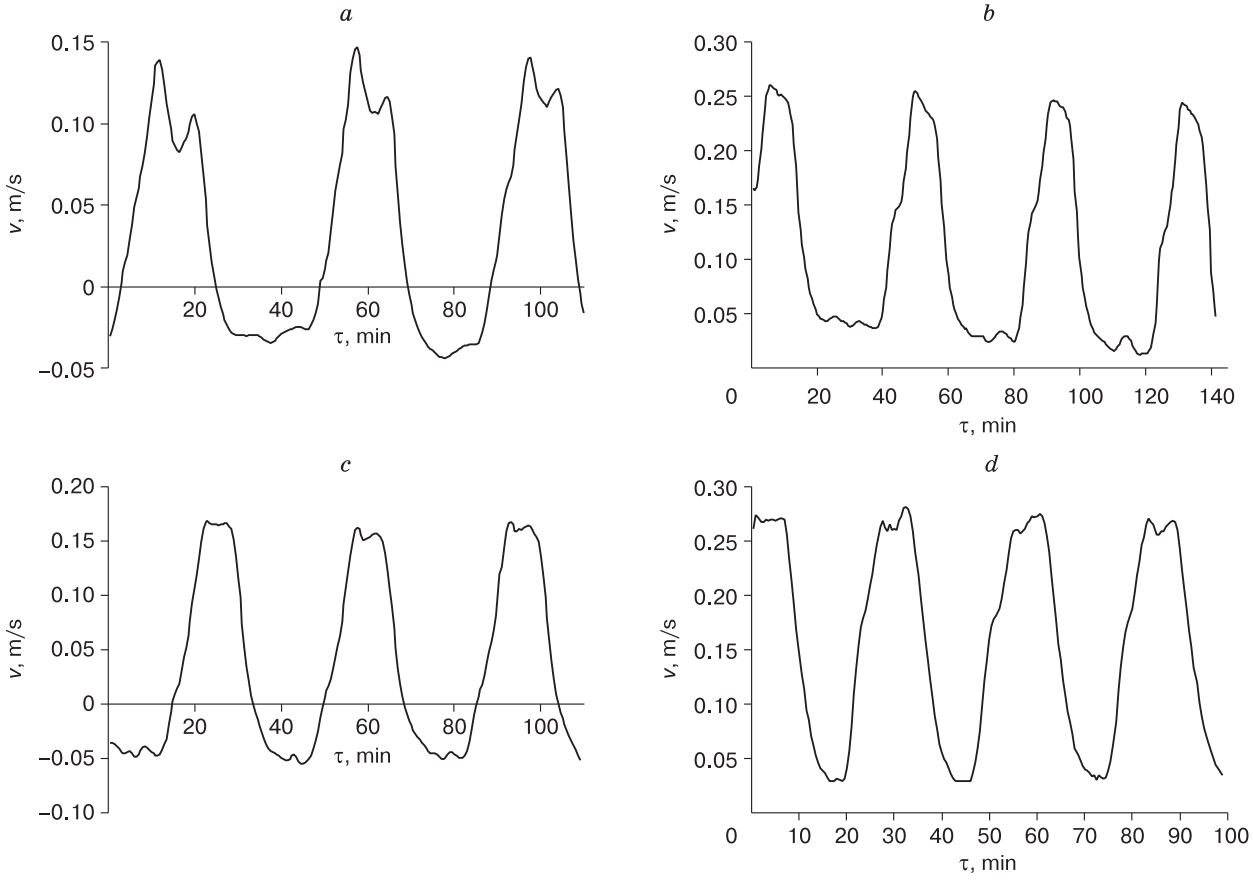


**Fig. 6. Fluid flow rate ($v$) at the condenser outlet as a function of time ($\tau$) under different heat outputs, a day after the system start.**

*a* – 0.734 kW; *b* – 1.05 kW; *c* – 1.51 kW; *d* – 2.05 kW.

$v$ = 0.1 m/s, simultaneously decreasing. We thus obtain: $\tau_0$ = 16 min, $\tau_1$ = 59 min, $\tau_2$ = 99.5 min, $\tau_3$ = 139.5 min. The periods that include times of peaks are: $T_1 = \tau_1 - \tau_0$ = 43 min (second peak); $T_2 = \tau_2 - \tau_1$ = 40.5 min (third peak); $T_3 = \tau_3 - \tau_2$ = = 40 min (fourth peak). Using the method described above, we decompose the Fourier series of the function shown in Fig. 6, *b*, according to formulas (5), (6), over a period containing times of the second, third, and fourth peaks. From the obtained functions $f_3$, $f_4$,

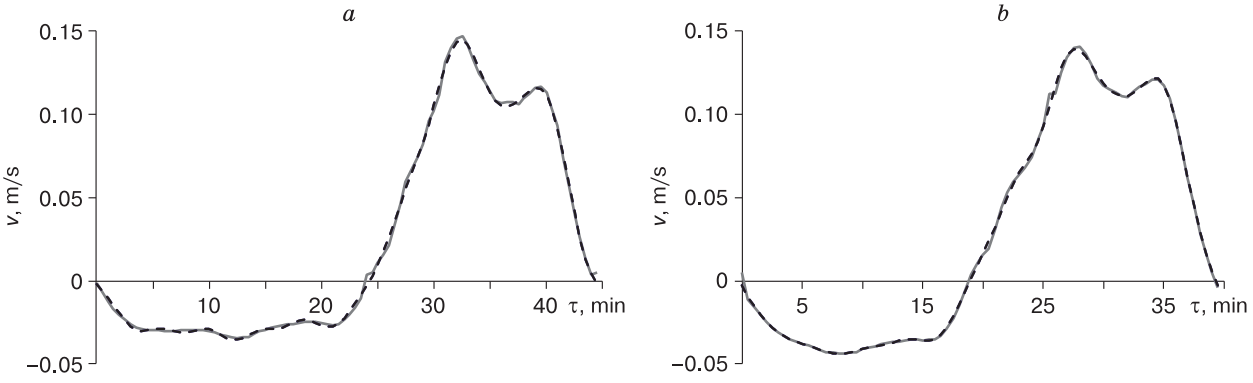


**Fig. 7. Correlation between the experimental fluid flow rates at the condenser outlet and calculated values for the middle (*a*) and right-hand (*b*) spikes (see Fig. 6, *a*).**

Experimental data are shown in solid line, dashed line is calculated (theoretical) data.

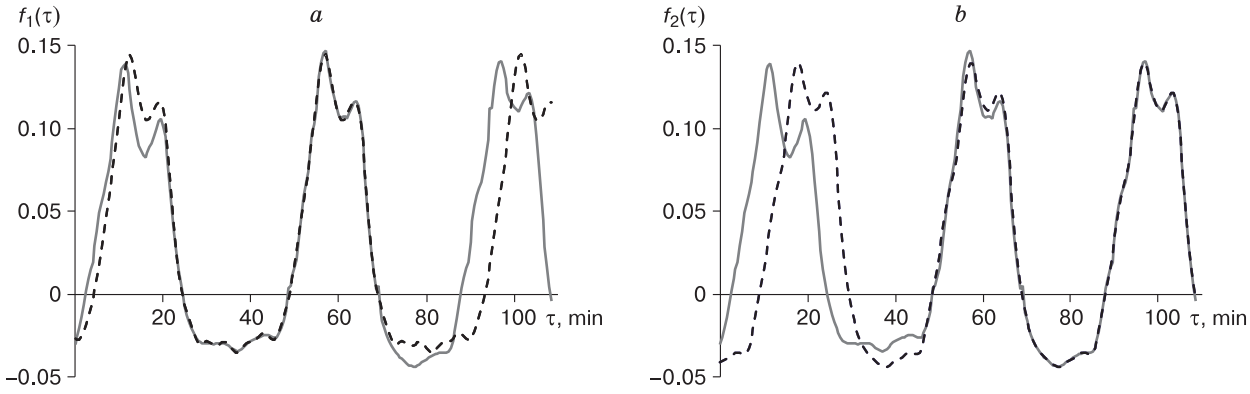


**Fig. 8. Functions $f_1$ (*a*) and $f_2$ (*b*) compared to the experimental data ($P$ = 0.734 kW).**

Experimental data are shown in solid line, dashed line is calculated (theoretical) data.

$f_5$ the function $f_4(\tau)$ that has the best fit is shown in Fig. 9.

For the purpose of another function decomposition (Fig. 6, *c*), let's consider three time values at which the function crosses the line $v = 0$ and simultaneously increases. We obtain: $\tau_0 = 14$ min, $\tau_1 = 49$ min, $\tau_2 = 84.5$ min; the period containing the first peak, $T_1 = \tau_1 - \tau_0 = 35$ min; and the period containing the second peak, $T_2 = \tau_2 - \tau_1 = 35.5$ min. Using the same technique, we decompose the Fourier series of the function shown in Fig. 6, *c* using formulas (5), (6), over a period containing times of the second, third, and fourth peaks. Among the obtained functions $f_6$ and $f_7$, the function $f_6(\tau)$ shown in Fig. 10 provides the best fit.

Decomposing the function shown in Fig. 6, *d* into a Fourier series requires considering three time values at which the function crosses the line $v = 0.1$ m/s and simultaneously decreases. We obtain: $\tau_0 = 10.5$ min, $\tau_1 = 38$ min, $\tau_2 = 65.5$ min, $\tau_3 = 93.5$ min. The periods containing time of the peaks are: $T_1 = \tau_1 - \tau_0 = 27.5$ min (second peak); $T_2 = \tau_2 - \tau_1 = 27.5$ min (third peak); $T_3 = \tau_3 - \tau_2 = 28$ min (fourth peak). We decompose the Fourier series of the func-

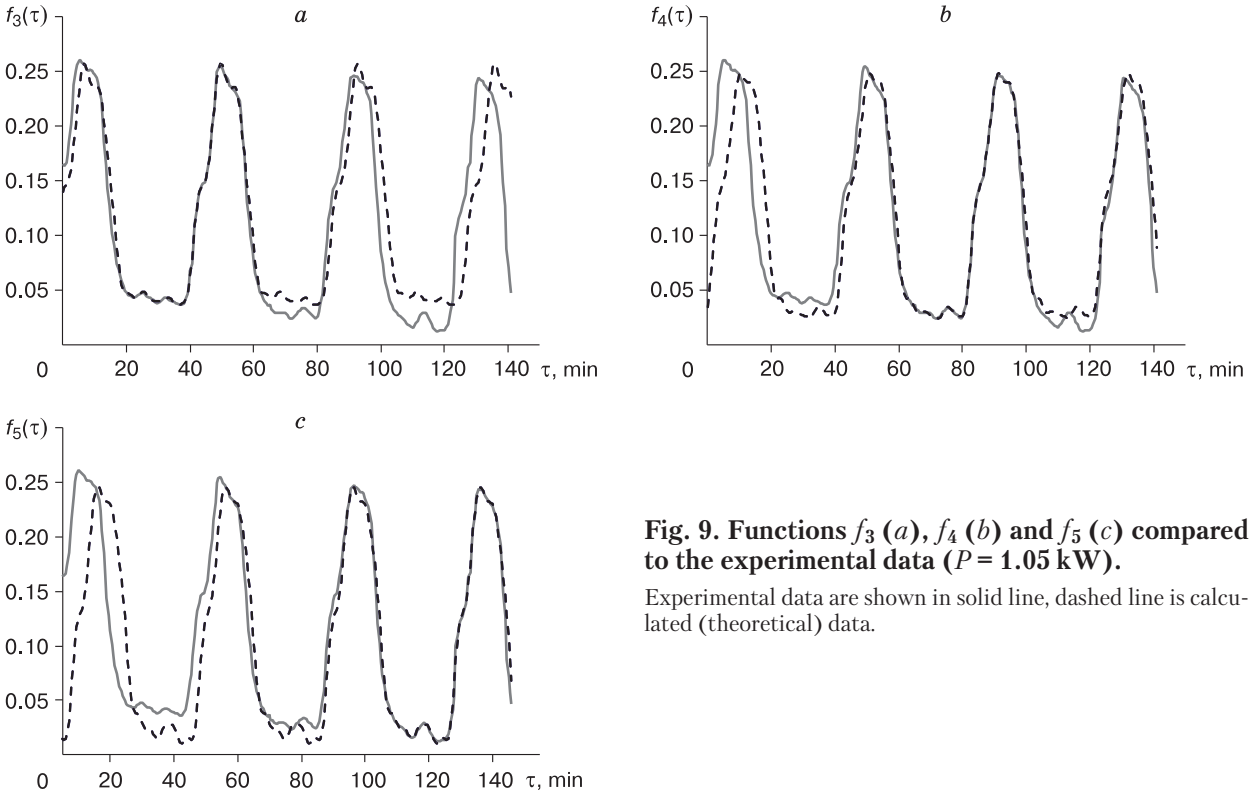


**Fig. 9. Functions $f_3$ (*a*), $f_4$ (*b*) and $f_5$ (*c*) compared to the experimental data ($P$ = 1.05 kW).**

Experimental data are shown in solid line, dashed line is calculated (theoretical) data.

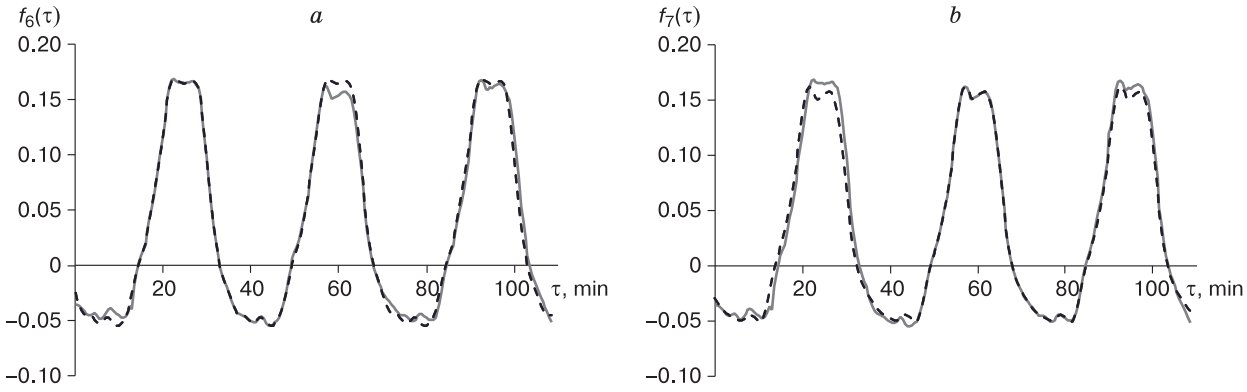


**Fig. 10. Functions $f_6$ ($a$) and $f_7$ ($b$) compared to the experimental data ($P$ = 1.51 kW).**

Experimental data are shown in solid line, dashed line is calculated (theoretical) data.

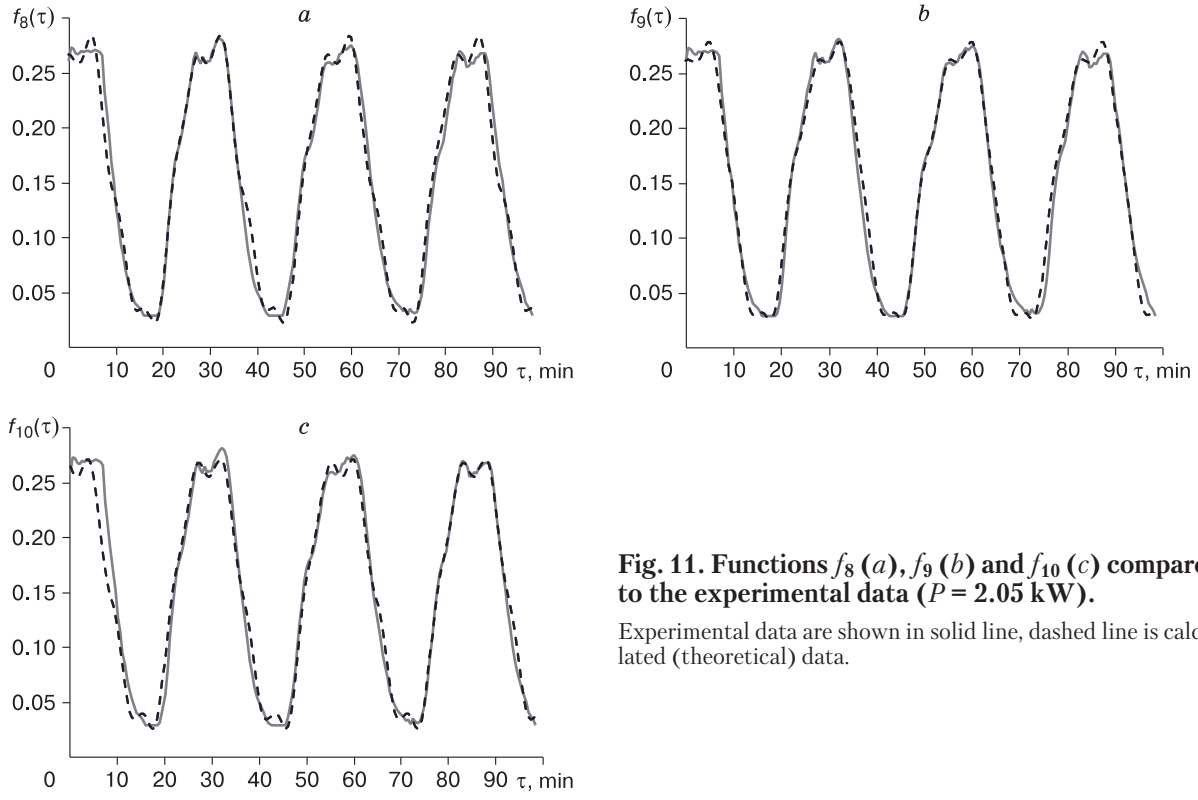


**Fig. 11. Functions $f_8$ ($a$), $f_9$ ($b$) and $f_{10}$ ($c$) compared to the experimental data ($P$ = 2.05 kW).**

Experimental data are shown in solid line, dashed line is calculated (theoretical) data.

Table 1. **Average fluid flow rate ($v$) at the condenser outlet for stable operation regime under high heat outputs ($P$) and oscillating counter-flow (left) and unidirectional fluid flow (right) in the oscillation minima**

| $P$, kW | $v$, m/s | $P$, kW | $v$, m/s |
|---|---|---|---|
| 0.734 | 0.0265 | 1.05 | 0.102 |
| 1.51 | 0.0366 | 2.05 | 0.155 |
| 2.07 | 0.059 | 3.62 | 0.126 |
| 3.62 | 0.126 | 6.25 | 0.164 |
| 6.25 | 0.164 | 7.89 | 0.183 |
| 7.89 | 0.183 | | |

tion shown in Fig. 6, $d$ using formulas (5), (6), and the period containing times of the second, third and fourth peaks. Of the two functions, $f_8$ and $f_{10}$, the function $f_8(\tau)$ shown in Fig. 11 provides the best fit.

The following runs were performed at high thermal power (heat outputs) received by the evaporator. At this, no fluctuations of the working liquid rate were observed at the condenser outlet. Results of the analysis of average flow rate of the working fluid at the condenser outlet under sustainable operation of the system and oscillating flow rate (on average, $0.5a_0$) are listed in Table 1.

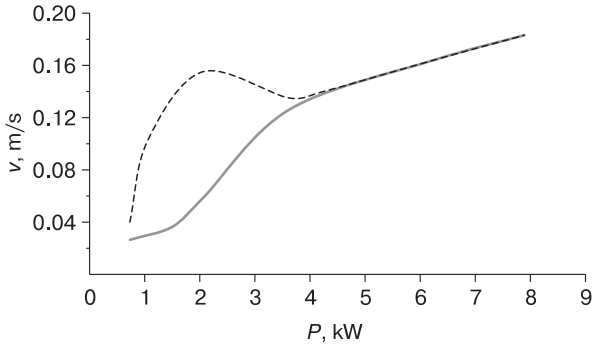


**Fig. 12. Working fluid flow rate at the condenser outlet ($v$) as a function of thermal power ($P$) received by evaporator.**

Solid line shows pulsating regime with a change in the fluid flow direction (counter-flow); dashed line is pulsating regime with unidirectional fluid flow (see Table 1).

Visualization of both dependencies approximated by spline is shown in Fig. 12. Given a total heat output is higher than 3.60 kW (11.84 W/m), the observed flow rate would correspond to stable operation regime (i.e. the curves overlap here).

## CONCLUSIONS

1. It is shown that a system charged with carbon dioxide as coolant will have better permafrost stabilization effect, as compared to a similar system using ammonia as the working fluid (coolant).

2. The three modes (regimes) of the working fluid flow shown to be inherent in the system are: stable (at high heat outputs); pulsating with a change in the fluid flow direction (counter-flow); and pulsating with unidirectional fluid flow. Under all the three regimes, the system operated and would effectively give up the heat from the evaporator to the outside ambient air.

3. It is shown that at thermal loads on the evaporator segment in excess of 3.60 kW (11.84 W/m), the observed working fluid flow will correspond to stable operation of the system. Using this value allows selecting the best system configuration, though this issue requires further investigations.

*The work was financially supported by "Provincial Academy" Autonomous Nonprofit Organization.*

## References

Anikin, G.V., Spasennikova, K.A., 2014. On the choice of refrigerating fluid for type "GET" systems for seasonal cooling. Earth's Cryosphere XVIII (2), 26–28.

Dolgikh, G.M., Okunev, S.N., 1989. Nature conservation measures, environment-friendly technologies, and equipment for development of new gas and condensate fields in the Yamal Peninsula. In: Research Activity Report. Giprotyumenneftegaz, Tyumen, 152 pp. (in Russian).

Ershov, E.D. (ed.), 1999. Fundamentals of Geocryology. Part 5. Engineering Geocryology. Moscow University Press, Moscow, 526 pp. (in Russian).

Farouki, O.T., 1986. Thermal Properties of Soils. Trans. Tech. Publications, Clausthal-Zellerfeld, Germany, 136 pp.

Feklistov, V.N., Dolgikh, G.M., Okunev, S.N., Pazderin, D.S., 2008. Investigation into HET thermosyphons for soil stabilization. In: Resources of Polar and Highland Areas. State and Prospects of Geocryology: Proc. Intern. Conf. Tyumen, Book 2, pp. 165–168.

Gorelik, J.B., 2015. Operation of two-phase thermosyphons with horizontal evaporator tubes: causes of instability. Earth's Cryosphere XIX (4), 74–83.

Holubec, I., 2008. Flat loop thermosyphon foundations in warm permafrost. In: Report submitted to the Government of the Northwest Territories, Asset Management Division. Department of Public Works and Services, and Public Infrastructure Engineering Vulnerability Committee, 83 pp.

Holubec, I., 2010. Geotechnical site investigation guidelines for building foundations in permafrost. In: Report submitted to the Government of the Northwest Territories. Department of Public Works and Services, Canada, 48 pp.

Ishkov, A.A., Anikin, G.V., Dolgikh, G.M., Okunev, S.N., 2018. Horizontal evaporator tube (HET) thermosyphons: physical-mathematical modeling and experimental data, compared. Earth's Cryosphere XXII (5), 51–56.

Long, E.L., 1963. The long thermopile. In: Proceedings of the First International Conference on Permafrost. Purdue University, US National Academy of Sciences, Purdue, pp. 487–490.

*Received October 28, 2019*
*Revised version received January 21, 2020*
*Accepted January 31, 2020*